

Water is a radiation protection agent for ionised pyrrole

Melby Johny,^{1,2,3} Constant A. Schouder,^{4,5} Ahmed Al-Refai,¹ Lanhai He,¹

Joss Wiese,^{1,2,6} Henrik Stapelfeldt,⁴ Sebastian Trippel,^{1,2,*} and Jochen Küpper^{1,2,3,6}

¹Center for Free-Electron Laser Science, Deutsches Elektronen-Synchrotron DESY, Notkestrasse 85, 22607 Hamburg, Germany

²Center for Ultrafast Imaging, Universität Hamburg, Luruper Chaussee 149, 22761 Hamburg, Germany

³Department of Physics, Universität Hamburg, Luruper Chaussee 149, 22761 Hamburg, Germany

⁴Department of Chemistry, Aarhus University, Langelandsgade 140, 8000 Aarhus C, Denmark

⁵LIDYL, CNRS, CEA, Université Paris-Saclay, 91191 Gif-sur-Yvette, France

⁶Department of Chemistry, Universität Hamburg, Martin-Luther-King-Platz 6, 20146 Hamburg, Germany

(Dated: 2023-04-07)

Radiation-induced damage of biological matter is an ubiquitous problem in nature. The influence of the hydration environment is widely discussed, but its exact role remains elusive. Utilising well defined solvated-molecule aggregates, we experimentally observed a hydrogen-bonded water molecule acting as a radiation protection agent for ionised pyrrole, a prototypical aromatic biomolecule. Pure samples of pyrrole and pyrrole(H₂O) were outer-valence ionised and the subsequent damage and relaxation processes were studied. Bare pyrrole fragmented through the breaking of C–C or N–C covalent bonds. However, for pyrrole(H₂O), we observed a strong protection of the pyrrole ring through the dissociative release of neutral water or by transferring an electron or proton across the hydrogen bond. Overall, a single water molecule strongly reduces the fragmentation probability and thus the persistent radiation damage of singly-ionised pyrrole.

INTRODUCTION

The damage of biological matter upon the interaction with UV radiation [1] or ionising radiation [2], such as x-rays [2, 3], γ -rays [4], and α -particles [5], or other charged particles [3, 6, 7] is a major environmental impact on living organisms [1, 2]. For instance, inner-shell-, inner-valence-, or outer-valence-ionised states can relax in various pathways that form cationic species, which can result in break up of the molecules [3, 8, 9]. In addition, recent studies show that one highly relevant mechanism of DNA strand breaks is *via* autoionisation or excitation caused by low-energy secondary electrons [3, 6, 7, 10].

Regarding the radiation damage of molecules, ionisation and excitation are similar: In both cases, vacancies are created in the occupied molecular orbitals, and this can lead to bond breaking. In the case of ionisation, the electron is directly transferred to the continuum, leaving the molecule, while excitation may result in the population of dissociative excited states [11]. Typical sources for single ionisation of biological matter in aqueous environments are deep UV radiation or the interaction with radicals, slow electrons, or ions [2, 3, 11, 12]. While deep UV radiation is efficiently blocked by the earth's atmosphere [13] it is omnipresent in outer space [14]. Harder, e. g., ionising, radiation penetrates the atmosphere.

Molecular assemblies such as clusters, droplets, and even large molecules like proteins in their natural solvation environment are known to allow for additional relaxation pathways due to intermolecular interactions [8, 15–23]. These pathways may lead to a protection of the molecule especially if the biomolecule is directly affected by the radiation [1]. On the other hand, secondary species originating from the ionisation of surrounding solvent molecules

can induce new pathways that lead to biomolecular destruction.

Hydrogen-bonded solute-solvent complexes allow for quantitative investigations of these effects [24–27]. One of the important electronic relaxation channels of such solvated-molecule clusters after x-ray ionisation, electron-impact ionisation, or α -particle irradiation was ascribed to intermolecular Coulombic decay (ICD) [8, 9, 24–26, 28]. This resulted in the formation of mainly charge-separated di-cationic complexes which undergo fragmentation *via* electrostatic repulsion. A competing ultrafast relaxation channel of hydrogen-bonded complexes after inner-shell ionisation, which may protect biomolecules, is intermolecular electron- or proton-transfer-mediated charge separation [21, 23, 26]. This was also observed following x-ray ionisation of the water dimer [27] and liquid water [29, 30].

To examine the influence of nano-hydration on the dynamics of biomolecules various studies using mass spectrometric techniques were performed [31–40]. These experiments can essentially be divided into three approaches: In the first approach one uses mass selective ion beam methods to extract individual clusters in the case of cationic and anionic samples [31, 32]. The initialisation of the dynamics, e. g. ionisation, is species unspecific which results in an undefined initial condition. For instance, it is not possible to avoid ionisation of the water as the initial step. The second approach of experiments utilises a localised initiation for the dynamics inside the cluster using, e. g., multi-photon ionisation [33–35] or slow electrons [36–38]. Here, however, experiments are done with mixed samples, e. g., various cluster sizes and isomers present in the molecular beam simultaneously. An unambiguous assignment of the fragments to a corresponding parent cluster is not possible. This is especially a problem in the case where

the isolated molecules and the clusters give rise to the same fragments. The third approach utilises neither a well-defined probe nor a localised trigger [39, 40].

A key ingredient for the indirect destruction pathways of biological matter is the radiolysis of water [12, 41, 42], likely because typically $\sim 3/4$ of a cell's volume comprises an aqueous environment [3, 12]. In this case, reactive cations, radicals, anions, or electrons are produced inside the water environment, which can trigger biomolecular fragmentation [2, 41–45]. In this context, numerous experimental studies claim that the hydration environment can either inhibit or enhance radiation-induced biological damage [4, 12, 32, 34, 37, 45–50]. This includes a recent study showing a relatively weak catalysis effect, i. e., an enhancement of radiation damage, due to water being present [38]. The details obviously depend on the nature of the ionising radiation and the specific potential energy landscape of the biomolecule in its hydration environment [2, 3].

Pyrrole, a heterocyclic aromatic molecule, is a UV-absorbing chromophore, e. g., in hemes and chlorophylls [51]. Pyrrole is also a subunit of indole, 3-methylindole, and tryptophan, which are of great relevance as the principal UV absorbers of proteins [52, 53]. The photophysical and photochemical properties of indole and pyrrole are sensitive to the hydration environment [54–59]: upon UV absorption these chromophores indirectly populate an excited ${}^1\pi\sigma^*$ state, which is repulsive along the N-H-stretching coordinate [52–54]. This triggers an ultrafast internal-conversion process to the ground state, essential for the photostability of proteins [60].

The pyrrole(H_2O) cluster has a well-defined structure with a hydrogen bond between pyrrole's N-H site and the water's oxygen [61]. This reflects the strongest interaction between pyrrole and surrounding H_2O in aqueous solution. H-elimination dynamics from the N-H site of pyrrole, mediated by the electronic excitation of the ${}^1\pi\sigma^*$ state [52, 62–64] or by vibrationally mediated photodissociation [65], was studied by time-resolved photoion and photoelectron spectroscopy. Theoretical calculations for electronically excited pyrrole(H_2O) clusters predicted electron transfer across the hydrogen bond without photodissociation of the pyrrole moiety [56, 66]. Direct ionisation from the HOMO and HOMO-1 orbitals of pyrrole [67, 68] and the HOMO orbital of pyrrole(H_2O) [69, 70] does not lead to fragmentation of the aromatic ring. However, the dissociation from excited cationic states of pyrrole led to molecular fragmentation [67, 68], and similar processes are expected for pyrrole(H_2O).

Here, we experimentally investigated the damage incurred in singly- and doubly-ionised pyrrole molecules and the effect of solvation by comparing the fragmentation pathways of bare pyrrole and microsolvated pyrrole(H_2O) heterodimers using the combination of pure samples of either species [70] and local, site-specific multi-photon ionisation. Our clean approach enables the systematic in-

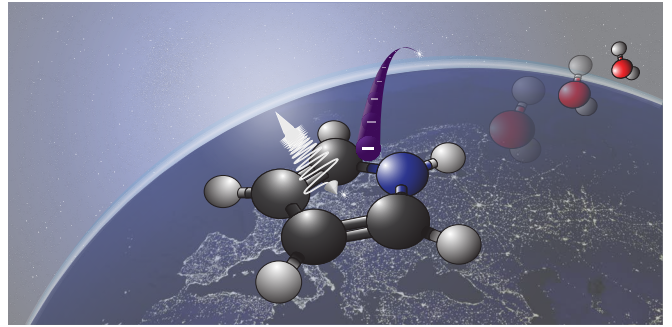


FIG. 1. Schematic representation of the ionisation scheme and radiation-protection mechanism in pyrrole(H_2O). Single ionisation of pyrrole(H_2O) is followed by its dissociation, with the leaving water molecule allowing the aromatic ring to stay intact without further fragmentation.

vestigation of the role of water solvent on the photophysics of pyrrole and for hydrated biomolecules in general.

A schematic representation of our ionisation strategy is represented in Figure 1. We mimicked the triggering of radiation damage through outer valence ionisation as it would naturally occur in secondary processes such as the interaction with slow electrons or UV photons. Pyrrole and pyrrole(H_2O) were site-specifically ionised by removing electrons from the highest-energy molecular orbitals, whose densities are predominantly localised on the aromatic ring as shown in Figure 7. This was achieved by strong-field ionisation using 800 nm laser pulses with a peak intensity of 10^{14} W/cm² and a pulse duration of 30 fs, see Methods for details. On one hand, valence ionisation of bare pyrrole resulted in extensive fragmentation, i. e., breaking of the aromatic ring. On the other hand, for singly-ionised pyrrole(H_2O) we mainly observed solely the breaking of the hydrogen bond with the water molecule leaving the intact pyrrole ring. In this case, breaking of the actual biomolecule is strongly suppressed.

RESULTS

Our comparison of the fragmentation dynamics of bare and microsolvated pyrrole built on the production of very pure molecular beams of pyrrole and pyrrole(H_2O), respectively; see Methods for details. The molecular beam had, in the case of pyrrole, a purity of ~ 95 %, with a ~ 5 % contamination by pyrrole dimer. The purity of the pyrrole(H_2O) beam was ~ 99 % with the main contamination being the water dimer.

Fragmentation dynamics of pyrrole

Figure 2 shows the time-of-flight mass spectrum (TOF-MS) and corresponding velocity-map images (VMIs) of all ions resulting from strong-field ionisation of pyrrole.

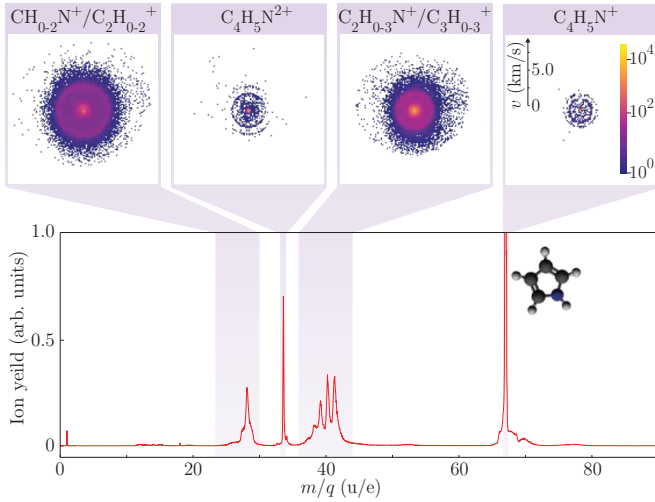


FIG. 2. Time-of-flight mass spectrum and corresponding velocity-map images of the ions generated by strong-field ionisation of pyrrole. The structure of pyrrole is given on the right of the lower panel. The colourmap and velocity scale holds for all velocity-map images.

All data were recorded simultaneously using a Timepix3 camera [71–73]. Rings in the VMIs occur for two-body Coulomb explosion, i. e., a charge-repulsion-driven fast breakup into two positively charged fragments. These fragmentation channels obey momentum conservation in the recoil frame. Low-kinetic-energy (KE) features correspond to intact parent ions or ions created from dissociative single ionisation. The data shows no signatures of three-body breakup beyond hydrogen atom/proton loss.

The most prominent feature in the TOF-MS is the narrow peak at $m/q = 67$ u/e, assigned to pyrrole⁺, on top of a broader pedestal. The peak corresponds to the sharp central dot in the corresponding VMI. The pedestal correlates with the rings in the VMI which are assigned to pyrrole⁺ from Coulomb explosion of the pyrrole dimer. The TOF-MS peak at $m/q = 33.5$ u/e and the central dot in the corresponding VMI are assigned to doubly-ionised pyrrole. Its pedestal in the TOF-MS and the corresponding rings in the VMI were attributed to pyrrole²⁺ from Coulomb explosion of multiply-ionised pyrrole dimer. In both cases 95 % of the signal strengths were in the central peaks, i. e., originated from the monomer.

The signals in the mass-to-charge regions $m/q = 24 \dots 30$ u/e and $m/q = 35 \dots 44$ u/e correspond to fragments from the breakup of the pyrrole ring. Some possible ionic products are labeled in Figure 2, in line with the mass peak assignment after electron-impact- and photoionisation of pyrrole [67, 74]. A clear assignment of the various individual peaks observed in the two mass regions to specific fragments was not possible due to overlapping signals and ambiguities in the construction of specific mass-to-charge ratios out of possible feasible fragments.

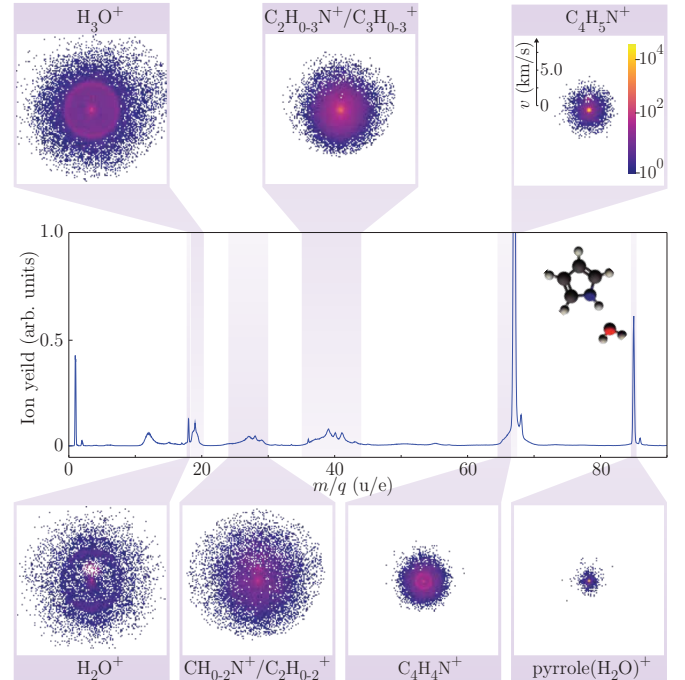


FIG. 3. Time-of-flight mass spectrum of pyrrole(H₂O) with the velocity-map images of the ions, which were recorded simultaneously after strong-field ionisation. Also shown are the structure of the dimer, sum formulas of all fragments, and the velocity ranges and colourmap for all velocity-map images.

The situation was further complicated by the fact that some fragments lost hydrogen atoms. However, proton loss after double ionisation was ruled out due to the lack of correlations between the detected protons and the fragments observed in the two mass regions. The small proton peak in the spectrum was attributed to initial charge states >2 , which are not further discussed in the current work. The structure at $m/q = 70$ u/e is assigned to contributions from larger clusters. The expected $m/q = 68$ u/e ¹³C-pyrrole isotopologues peak is suppressed due to the strong parent ion signal, see Methods. Intense central peaks in the VMIs correspond to fragments from dissociative ionisation of singly-charged pyrrole. Rings in the VMIs, contributing ~ 30 % of the total ion count, correspond to fragments from Coulomb explosion of doubly-charged pyrrole. The Coulomb explosion signals of the $m/q = 24 \dots 30$ u/e and $m/q = 35 \dots 44$ u/e mass regions are correlated for the double ionization of bare pyrrole, as confirmed by kinetic-energy-selected coincidence maps and momentum conservation.

Fragmentation dynamics of pyrrole(H₂O)

Figure 3 shows the TOF-MS and VMIs of all ions resulting from strong-field ionisation of pyrrole(H₂O). Again all data were recorded simultaneously using the Timepix3

detector. All VMIs exhibit a central low-KE part due to single ionisation as well as sharp or diffuse higher-KE signals.

The peak at $m/q = 85$ u/e, with a central dot in the VMI, corresponds to the pyrrole(H_2O)⁺ parent ion. The strongest peak in the TOF-MS is again at $m/q = 67$ u/e, the pyrrole-monomer cation, which resulted from the dissociation of the hydrogen bond in singly-ionised pyrrole(H_2O). This is confirmed by its broader KE distribution in the VMI owing to recoil from the momentum conservation with the leaving neutral water molecule. Furthermore, no correlations were found in the PIPICO map between singly charged pyrrole ions itself suggesting that the contributions from pyrrole homo dimers are negligible.

The peaks at $m/q = 66$ u/e and $m/q = 19$ u/e correspond to $\text{C}_4\text{H}_4\text{N}^+$ and H_3O^+ , respectively. Both fragments exhibit sharp rings in their VMIs, with correlated ions that obeyed momentum conservation, demonstrating a two-body Coulomb explosion break-up channel of pyrrole(H_2O) including a proton transfer from pyrrole to water. A weaker H_2O^+ channel, $\sim 3/4$ of which originates from pyrrole(H_2O) whereas the remaining signal can be attributed to the water dimer, shows the direct charge-separating breakup of pyrrole(H_2O)²⁺ across the hydrogen bond.

As for pyrrole, fragments within the regions $m/q = 24 \dots 30$ u/e and $m/q = 35 \dots 44$ u/e were detected due to the breakup of the aromatic ring. However, they showed broad structureless distributions in the VMIs which were not correlated with each other. The high-KE ions in these regions originate from pyrrole(H_2O)²⁺ after three-body fragmentation processes. These channels involved H_3O^+ as a second ionic partner, as well as a neutral fragment. The small peak at $m/q = 36$ u/e was attributed to singly-ionised water dimer ($(\text{H}_2\text{O})_2$) [75].

DISCUSSION

Overall, single- and double-valence ionisation of pyrrole led to a significant breakup of the aromatic ring, in addition to the formation of singly- or doubly-charged parent ions. Single ionisation of pyrrole into the ²A₂ ground state and the ²B₁ first excited state of the cation led to the formation of a stable parent ion [67, 68]. Single ionisation also caused fragmentation of the pyrrole moiety through various dissociative pathways, which resulted in low-kinetic-energy ions. This was due to ionisation into diffuse bands of excited electronic states of the cation with energies in the range of 12...15 eV, i. e., around 4 eV above the ground-state energy of the cation [67, 68, 76–78]. With Koopmans' theorem, the energies of these excited states match well with the ionisation energies of HOMO-2 to HOMO-6 orbitals of the pyrrole molecule [67]. Double ionisation caused fragmentation of the aromatic ring

driven by Coulomb explosion.

Surprisingly, the scenario was very different for singly- and doubly-ionised pyrrole(H_2O). New relaxation pathways emerged due to the hydrogen bond with the water molecule – despite the predominantly localised ionisation with the removal of electrons from pyrrole's π orbitals. For example, in the case of singly-ionised pyrrole(H_2O), we observed a strong dissociation channel for the hydrogen bond, i. e., the loss of neutral water, which protected the pyrrole ring from fragmentation. Furthermore, after double ionisation additional Coulomb-explosion channels appeared for pyrrole(H_2O) compared to pyrrole, such as the H_3O^+ channel with its counter ion $\text{C}_4\text{H}_4\text{N}^+$. Both fragments showed sharp rings in the corresponding VMIs, demonstrating that the pyrrole ring was left intact with only a proton transferred to the water moiety. Additionally, two body Coulomb-explosion channels of pyrrole(H_2O) in the regions $m/q = 24 \dots 30$ u/e and $m/q = 35 \dots 44$ u/e, i. e. clear rings, were absent and the uncorrelated signal was much weaker than the strong signals observed for the pyrrole monomer. In total, the fragmentation pathways were significantly influenced, i. e., fragmentation of the pyrrole ring was strongly reduced by the attached single water molecule.

Single ionisation of pyrrole(H_2O) into the ground state of the cation created intact parent ions with the charge localised on the aromatic moiety. The binding energy of the cationic dimer was determined to 670 meV [69]. The energy of the first excited state is expected to be roughly 1 eV above the ground state of the cation, as in the case of the pyrrole monomer [67, 76]. In the TOF-MS of pyrrole(H_2O), Figure 3, the dominant peak was $m/q = 67$ u/e, so a dissociation product of pyrrole(H_2O). The pyrrole cation arose from the dissociation following single ionisation of pyrrole(H_2O). Assuming a similar ionisation cross-section for pyrrole and pyrrole(H_2O) into the first electronically excited state of the cation led to the conclusion that this state of pyrrole(H_2O) was dissociative. Otherwise the pyrrole(H_2O) spectrum would be dominated by pyrrole(H_2O)⁺. Therefore, the aromatic ring was protected after ionisation into the ground and the first excited state of the pyrrole(H_2O) cation. We also observed similar aromatic ring fragmentation products for pyrrole(H_2O), as in the case of pyrrole, from the above-mentioned diffuse dissociation band [67, 76]. However, the relative intensities between stable aromatic rings versus fragmentation channels varied significantly for the monomer and the heterodimer, leading to a higher ring fragmentation probability for the former.

To unravel the influence of the microsolvation on the radiation-induced damage and to quantify the degree of protection for ionised pyrrole in the presence of a single water molecule, we normalised the ion yields for the pyrrole and pyrrole(H_2O) species with respect to each other. We normalised both species based on their total single-ionisation ion yield by assuming the single-ionisation cross-

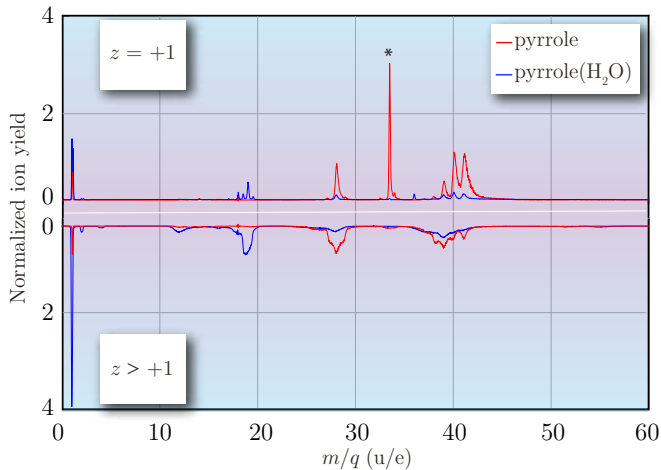


FIG. 4. Comparison of the normalised TOF-MS of pyrrole (red) and pyrrole(H₂O) (blue). The number of charges created on the system after strong-field ionisation is denoted by z . The upper panel corresponds to an initial charge state $z = +1$. The peak marked with the asterisk corresponds to intact C₄H₅N²⁺ from double ionisation of pyrrole. The lower section is for the charge states $z > +1$. Signals for $m/q = 2 \dots 14$ u/e in the lower section originated from initial charge states with $z > +2$.

section to be the same. This is justified by the similarity of laser-intensity-dependent single-ionisation ion yield for the two species as described in the Methods. Furthermore, the single, double, and higher-order ionisation channels were separated to provide a direct comparison of the fragmentation yields for both species as a function of the initial charge state. Corrections for saturation effects in detector areas with high count rates were statistically taken into account, see Methods. In addition, the fragmentation channels were classified into ring-fragmenting and ring-protecting channels.

The momentum maps for the specific mass-to-charge regions were taken into account in order to separate single, double, and higher-order ionisation channels. Almost all VMIs shown in Figure 2 and Figure 3 had contributions from ions with low as well as with high kinetic energy. We attribute the low-KE ions to single ionisation and the high-KE ions to double or higher-order ionisation, respectively. Gating on the momenta with $p < 30$ u km/s resulted in a normalised mass spectrum (NORMS), which is a composition of single-ionisation channels and the doubly charged parent ion channel that also exhibits low kinetic energy. Gating on the momenta with $p > 30$ u km/s resulted in a NORMS for the higher-order ionisation channels. The resulting normalised gated time-of-flight mass spectra for pyrrole and pyrrole(H₂O) are shown in Figure 4 for $m/q = 0 \dots 60$ u/e, which contain all ring-breaking fragments. The upper panel corresponds to the single-ionisation channels ($z = +1$), whereas the lower panel corresponds to double ($z = +2$) or higher ($z > +2$)

ionisation channels.

Both species showed similar fragmentation products, especially in the mass-to-charge regions $m/q = 24 \dots 30$ u/e and $m/q = 35 \dots 44$ u/e, which were the channels arising from the breaking of the pyrrole ring. However, they vastly differed in the specific ion yield and we observed a significant reduction of fragments arising from ring fragmentation for pyrrole(H₂O) than for pyrrole for single ionisation. For both, pyrrole and pyrrole(H₂O), the contributions in the NORMS for $z \geq +2$ in the region $m/q = 15 \dots 60$ u/e were dominated by double ionisation. This includes the large differences in the region $m/q = 18 \dots 19$ u/e where hydronium and water ions are formed. The contributions from triple ionisation were statistically estimated to less than 5 % and are thus negligible, see Methods. Furthermore, the NORMS peaks in the region $m/q = 1 \dots 14$ u/e originated from charge states with $z > +2$, confirmed by a covariance analysis. In the case of higher-order ionisation, i. e., $z > 2$, a direct comparison of the ion yield of pyrrole and pyrrole(H₂O) from the NORMS was not feasible due to the complex fragmentation processes and overlapping fragmentation channels.

To estimate the extent of fragmentation protection after single and double ionisation of pyrrole in a microsolvated environment, the observed fragmentation channels were classified into ring-breakup and ring-protection channels. Based on this, the ring-fragmentation probability is defined as $P = N_b/N_{\text{total}}$ with the number of fragments where the ring is broken N_b and the total ion yield N_{total} .

First, we considered ring-breakup and ring-protection channels following single ionisation of pyrrole and pyrrole(H₂O). For pyrrole, the parent ion was considered as a channel leaving the molecule intact. For single ionisation of pyrrole(H₂O), in addition to the parent ion, the dominant ring-protection channel was the dissociation of the hydrogen bond, i. e., the loss of neutral water. Furthermore, the dissociative single-ionisation processes resulting in low-KE ions of H₂O⁺, H₃O⁺, and C₄H₄N⁺, prevented the aromatic ring from fragmentation. All other low-KE ions in the mass-to-charge region $m/q = 15 \dots 60$ u/e were considered as ionic products that originated from the fragmentation of the aromatic ring. The ring-fragmentation probabilities for pyrrole and pyrrole(H₂O) after single ionisation were then determined by counting the ions in the momentum-map images with a gating specifically on the low-KE part in the specific mass-to-charge regions. The projection of ions from higher charge states ($z = +2$) into the center of the momentum-map images was estimated statistically, see Methods, and this contribution was subtracted.

We estimated the ring-fragmentation probability individually for pyrrole and pyrrole(H₂O) to 31 % and 6 %, respectively. Figure 5 provides a sketch of the corresponding potential-energy surfaces of pyrrole⁺ and pyrrole(H₂O)⁺ with the resulting products and their probabilities. Single

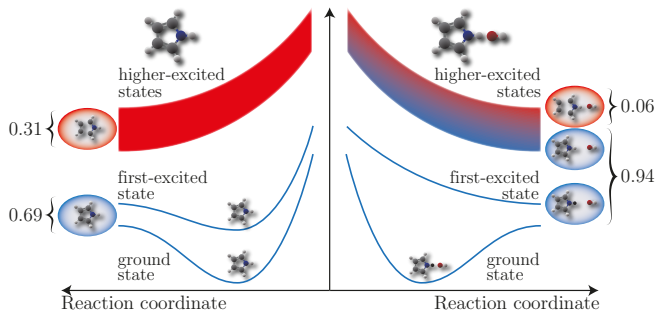


FIG. 5. Schematic representation of the potential energy surfaces and the first dissociation band of pyrrole⁺ and pyrrole(H₂O)⁺ together with the ring-protection and ring-breaking probabilities. Ring-protection and ring-breaking channels are represented by blue and red colours, respectively. In the case of pyrrole(H₂O)⁺ additional relaxation pathways emerged through the cleavage of the hydrogen bond for the first dissociation band. For simplicity, only one of the observed fragments is shown for each dissociation pathway.

ionisation of pyrrole into the ground and first excited state of the cation led to the formation of a stable parent ion, pyrrole⁺ [67, 68]. The ionised molecule underwent fragmentation through the higher excited cationic states [76], whose probability was 31 %. In the case of pyrrole(H₂O), single ionisation into the ground state resulted in a stable parent ion, pyrrole(H₂O)⁺ [69]. The first excited state of pyrrole(H₂O)⁺ dissociated the heterodimer into a pyrrole⁺ and neutral water. For the higher excited states of pyrrole(H₂O) a reduction in the ring fragmentation probability was observed. This was due to dissociative channels, where the water is leaving neutrally. Obviously, for the pyrrole monomer such channels do not exist.

Overall, the ring-fragmentation probability of pyrrole following single ionisation is reduced by a factor of approximately $31/6 = 5.2$ in pyrrole(H₂O) compared to pyrrole. Based on the observation of reduced fragmentation for pyrrole(H₂O) and the assumption of a similar cross section for single ionisation, we can infer that neutral molecules can be protected against radiation damage through outer-valence ionisation by solvation even with a specifically-bound single water molecule.

To shed light on radiation damage effects after double ionisation, we classified the channels following double ionisation of pyrrole and pyrrole(H₂O). For pyrrole, the only ring-protecting channel was the formation of a (meta)stable doubly-charged parent ion, C₄H₅N²⁺, marked by the asterisks in the upper panel of Figure 4. All other channels broke the aromatic ring. The dominant ring protection channel for the pyrrole(H₂O)²⁺ was the intermolecular proton transfer from the N–H site of the pyrrole moiety to the water moiety, producing H₃O⁺ and C₄H₄N⁺. A second channel was an electron transfer process across the hydrogen bond, which led to the formation of C₄H₅N⁺ and H₂O⁺. All other double-ionisation chan-

nels broke the aromatic ring, but in our experiment these were minor contributions. The ring-fragmentation probability for pyrrole and pyrrole(H₂O) after double ionisation was determined by counting ions in the high-KE part of the momentum-map images while taking into account that two ions might have been produced after double ionisation, leading to two hits in the corresponding momentum maps for a single fragmentation event; the finite detection efficiency of 0.5 for each ion was statistically taken into account. This led to a similar ring-fragmentation probability after double ionisation for pyrrole(H₂O), $P = 0.72 \pm 0.04$ and pyrrole, $P = 0.78 \pm 0.04$. Furthermore, we extracted a similar double-ionisation cross-section within our model, see Methods. This observation is consistent with our previous assumption that the cross sections for single ionisation are similar for both species.

CONCLUSION

We demonstrated that a single water molecule strongly protects the pyrrole molecule from fragmentation after single ionisation. Furthermore, we observed similar ring-fragmentation probabilities for pyrrole and pyrrole(H₂O) in the case of double ionisation. These quantitative studies were enabled by the production of pure samples of the bare molecule as well as the microsolvated complex and by the use of the versatile Timepix3 detector.

Singly-ionised pyrrole underwent radiation-induced damage through the breaking of, typically two, C–C or N–C bonds. Notably, the dissociation mechanisms after single ionisation of pyrrole(H₂O), through breaking of the intermolecular bond or by transferring an electron or proton across this hydrogen bond, strongly reduces the ring breaking probability by a factor of 5.2. We inferred that solvation effects also provided radiation protection for the neutral pyrrole(H₂O) system.

The radiation protection mechanisms for excited chromophores were studied both experimentally and theoretically [53, 54, 59, 60, 79]. Our study showed that this protective effect observed for solvated chromophores is also valid after ionisation.

Following double ionisation similar ring-fragmentation probabilities were observed for pyrrole and pyrrole(H₂O). In the microsolvated system, intermolecular proton- and electron transfer processes occurring across the hydrogen bond increased the redistribution of charges, initially created in the pyrrole ring, to the water molecule. This charge-distribution was observed through the formation of H₂O⁺ and H₃O⁺, where the counter ion is either an intact ring or a ring-fragmentation product.

We employed strong-field ionisation for the removal of electrons from the low-binding-energy molecular orbitals, which are localised on the pyrrole moiety in the monomer as well as the microsolvated systems. This process mimics the ionisation by slow secondary electrons in aqueous

systems, such as cells, as well as ionisation through VUV radiation – which both typically create singly-charged molecules since these ionisation processes access the same potential energy surfaces and therefore dissociative states.

Our results provide a test case of how an aqueous micro-solvation environment can strongly reduce the radiation damage of biological molecules induced by ionising radiation as well as the biologically important process of secondary effects of ionising radiation, where single outer-valence ionisation of the biomolecular chromophore is the scenario. Furthermore, the doubly-ionised systems in our experiment resemble to a large extent the fate of a molecule after Auger decay processes subsequent to direct core-shell ionisation [8, 9].

Biomolecules and proteins in nature are actively solvated by the surrounding water molecules, which allow for efficient charge redistribution to the solvent environment through electron- and proton transfer pathways quantified here. In aqueous solution, the loss of the attached – neutral, ionised, or protonated – water could easily be repaired by the many solvent molecules around. Our analysis of the protection in pyrrole(H_2O) provides a quantitative analysis of radiation protection and serves as the basis for further detailed investigations regarding the role of the solvent environment on the radiation damage of biomolecules.

METHODS

Experimental Setup

Details of the experimental setup were described elsewhere [80]. A pulsed valve was operated at 100 Hz to supersonically expand a few millibars of pyrrole (Sigma Aldrich, > 98 %) and traces of water in ~ 90 bar of helium into vacuum. The resulting molecular beam contained atomic helium, individual pyrrole and water molecules, and various aggregates thereof. The electric deflector was used to create pure samples of pyrrole(H_2O) with a typical purity close to 100% [70, 81]. Pyrrole and pyrrole(H_2O) were strong-field ionised by 800 nm laser pulses with linear polarisation, a duration of ~ 30 fs, focused to $\varnothing \approx 35$ μm (full width at half maximum intensity) with a peak intensity of $\sim 1 \times 10^{14}$ W/cm^2 . The ions generated were extracted perpendicular to the molecular beam and laser propagation directions using a velocity-map-imaging spectrometer (VMIS). All ions were detected using a position- and time-sensitive detector consisting of a micro-channel plate (MCP) in combination with a fast phosphor screen (P46). A visible-light-sensitive Timepix3 detector [71, 82] in an event-driven mode recorded all signals, which were stored and centroided using our homebuilt pymepix software [72].

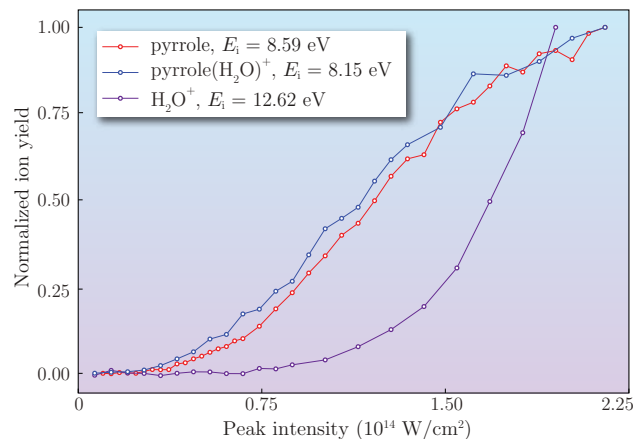


FIG. 6. Single-ionisation yields for pure samples of pyrrole (red), pyrrole(H_2O) (blue), and water (purple) measured at different laser peak intensities. All curves are normalised to their highest ion yield observed.

Normalisation of the mass spectra

The normalisation of the TOF-MS was necessary due to the different densities of the two species, pyrrole and pyrrole(H_2O), in the molecular beam. Due to the very similar first ionisation energies (E_i) of pyrrole and pyrrole(H_2O) the ionisation probabilities for both species are also very similar. The calculated (HF/MP2-aug-cc-pVTZ using GAMESS-US) first vertical E_i of pyrrole and pyrrole(H_2O) are 8.59 eV and 8.15 eV, respectively. To quantify the relative ionisation probability experimentally [83, 84] the ion yield as a function of the laser peak intensity was measured for the single-ionisation channel for pyrrole, pyrrole(H_2O), and water, see Figure 6. Here, the ion yield from each pure species is normalised to its value for the highest laser intensity. In the low-intensity region, $1\text{--}8 \times 10^{13}$ W/cm^2 , for pyrrole only the parent ion was observed. A saturation intensity for the parent ion signal of $\sim 6 \times 10^{13}$ W/cm^2 was obtained from the measured low-intensity ion-yield curve. For pyrrole(H_2O) we summed the signals for parent ion and pyrrole $^+$ [70], which yielded a saturation intensity for single ionisation of $\sim 4.5 \times 10^{13}$ W/cm^2 . Based on the similar saturation intensities and the very comparable intensity dependence of the ionisation yields, Figure 6, we assumed similar single-ionisation cross-sections and normalised the TOF-MS of pyrrole and pyrrole(H_2O) using a normalisation factor of 3.33 ± 0.1 . This normalisation factor is identical to the relative number densities of pyrrole and pyrrole(H_2O) beam.

For the ionisation of water, we obtained a very different intensity dependence and saturation intensity, which was determined as $\sim 1.4 \times 10^{14}$ W/cm^2 . This is consistent with the larger E_i of 12.62 eV [85] and further demonstrates the similarities in the ionisation cross sections of pyrrole

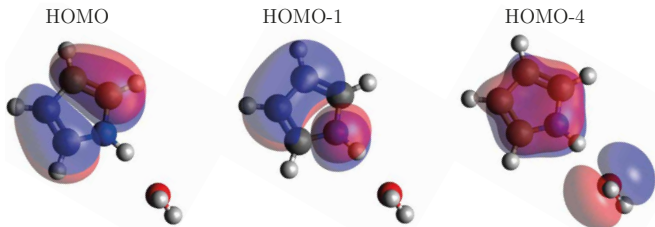


FIG. 7. Molecular orbital picture of HOMO, HOMO-1, and HOMO-4 for the geometry optimised ground state structure of the pyrrole(H_2O).

and pyrrole(H_2O).

Highest occupied molecular orbitals of pyrrole(H_2O)

The molecular orbitals calculated (GAMESS-US, HF/MP2-aug-cc-pVTZ) for the geometry-optimised ground state structure of pyrrole(H_2O) are shown in Figure 7. The electron densities of HOMO to HOMO-3 are localised on the aromatic ring. The highest-energy bound molecular orbital with significant density on the water moiety is HOMO-4. This orbital has an energy that is 6.5 eV lower than the HOMO. Therefore, under the applied laser intensities ionisation from this orbital can be neglected [86] and localised ionisation of pyrrole(H_2O) at the pyrrole moiety can be safely assumed.

Double-ionisation yield

We compared the absolute total ion yield of the monomer and the microsolvated system after double ionisation. This double-ionisation ion yield was indicated qualitatively through the comparison of the ion signals in the NORMS in Figure 4. However, a direct comparison of the yields in the TOF-MS was not straightforward due to the complex fragmentation pathways and the overlap of higher-order ionisation channels. Therefore, to quantify this, we counted the ions in the normalised momentum maps of the specific channels originating from double ionisation of pyrrole and pyrrole(H_2O). The normalisation was done using the extracted relative number density ratios between these two species, which was based on the assumption of similar single-ionisation cross-section for both species. The direct comparison of the total double-ionisation yields revealed a reduction of the total ion yield of pyrrole(H_2O), with respect to pyrrole, by a factor of 1.22 ± 0.3 . Thus, we concluded that the double-ionisation cross-section is also similar for pyrrole and pyrrole(H_2O) within the errors of our estimation model.

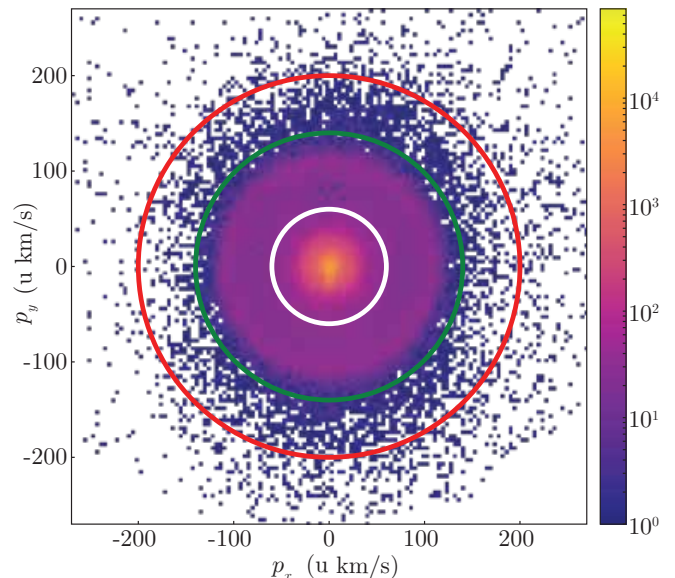


FIG. 8. The momentum map for all ions detected within a mass-to-charge region $m/q = 35 \dots 45$ u/e is shown. Marked circles with specific radii in the momenta map represent edges for single, double, and triple ionisation, respectively.

Triple-ionisation contributions

To estimate the contributions of individual ions over a given mass-to-charge range from the measured 2D projection of the 3D momenta, we made specific cuts in these experimental momentum maps in order to isolate contributions from single, double, and triple ionisation processes.

The measured momentum map for $m/q = 35 \dots 45$ u/e is shown with Figure 8 as an example. Circles indicate corresponding cuts in the 2D projection of the 3D momentum sphere formed from each ionisation process: The white circle with a radius of $p_r = 60$ u km/s represents the edge of the momentum for dissociative single ionisation, the green circle with $p_r = 140$ u km/s corresponds to the maximum momentum of ions from Coulomb explosion following the double ionisation, and the red circle with $p_r = \sqrt{2} * 140 \approx 200$ u km/s is the maximum momentum of ions from triple ionisation, assuming a two-body fragmentation into a singly-charged and a doubly-charged ion.

The total ion count corresponding to the disks defined by these specific radii and the signal in the two outer rings are provided in Table I. Areas of the specific disks and rings are also given. Ion counts inside the outer ring, $140 < p_r < 200$, correspond to triple ionisation without contribution from single and double ionisation. However, the middle ring, $60 < p_r < 140$, represents the double-ionisation channels and it has contributions from triple ionisation; similarly, the innermost disk, $0 < p_r < 60$, representing single ionisation has contributions

radius p_r	ion counts in disk	ion counts in ring	area of disk/ π	area of ring/ π
60	167522	167522	3600	3600
140	225860	58338	19600	16000
200	229120	3260	40000	20400

TABLE I. Total ion counts as well as the areas of disks and rings within specific radii chosen in the momenta map.

charge state	ion counts	ion counts/area
+1 (single)	$167522 - 3.486 \cdot 3600 - 0.1598 \cdot 3600 = 154397$	$154397/3600 = 42.89$
+2 (double)	$58338 \cdot (19600/16000) - 0.1598 \cdot 19600 = 68332$	$68332/19600 = 3.486$
+3 (triple)	$3260 \cdot (40000/20400) = 6392$	$6392/40000 = 0.1598$

TABLE II. Number of ion counts per area of each disk, and the estimated number of ions formed after the single, double, and triple ionisation, respectively.

from ions originating in double and triple ionisation. The corrected total number of ions from single, double, and triple ionisation are provided in Table II assuming a flat ion distribution in the inner part of the corresponding rings and disks. The relative contribution of the ion yield from the triple-ionisation process to the total ion yield in the given mass-to-charge region is $< 5\%$, i. e., negligible.

Determination of real ion numbers taking into account detector saturation

Here, the connection between the measured number of ions N_{det} and the real number of ions produced N_{real} taking into account saturation effects of the detection system are discussed. The saturation effects appear, e. g., for the parent ions, pyrrole and pyrrole-water, due to the small areas on the detector where these ions are detected. The small areas are accounted for the fact that the spectrometer was operated in VMI conditions in combination with the translational molecular beam temperature below 1 K. Furthermore, all parent ions arrive on the detector at the same TOF within the temporal resolution of the Timepix3 camera. This makes it impossible to determine the real number of parent ions per shot by counting since only a single event is detected at an instant of time by our detection system. Assuming a Poissonian distribution $P_\lambda(N_{\text{real}})$ of the real ions created, however, allows to estimate the real number of ions N_{real} from the detected number of ions N_{det} . Table III summarises the numbers and probabilities of various channels. The first column indicates the parent system under investigation. The corresponding ions are listed in the second column including the fragments. The corresponding number of laser shots are denoted with N_{shots} . The detected hit rate per shot $R_{\text{det}} = N_{\text{det}}/N_{\text{shots}}$ indicates the probability to detect an event for a single laser shot per channel. The probability to detect 0 ions within a laser shot is given by $P_\lambda(0) = 1 - R_{\text{det}}$. This value can be used to determine the mean number of ions

per shot $\lambda = -\ln(P_\lambda(0))$ according to the Poissonian distribution. The real number of ions N_{real} is then given by $N_{\text{real}} = N_{\text{shots}}\lambda$. For the ring fragmentation channels, we set $N_{\text{real}} = N_{\text{det}}$ due to the larger spatio-temporal volume covered by these ions on the detector. The ring fragmentation probability for pyrrole and pyrrole(H_2O) taking into account saturation effects of the detection system is therefore given by $P_{\text{P}} = (548485 + 241298)/241298 = 3.273$ and $P_{\text{PW}} = (1301176 + 159591 + 91799)/91799 = 16.912$, respectively. This gives rise to a ring protection factor given by $P = P_{\text{PW}}/P_{\text{P}} = 16.912/3.273 = 5.167$.

Pyrrole and pyrrole-water isotopologue peaks

The missing isotopologue peak for pyrrole is attributed to the dead time in the order of μs of the Timepix3 camera in combination with the relatively high detection rate per shot given by $R_{\text{det}} = 0.8688$ (see Table III) and the finite spatio-temporal resolution. The natural abundance of C_{13} isotope is in the order of 1.1%. This results in an expected relative peak height in the order of 4.5% for the C_{13} parent ion peak due to the 4 carbon atoms present in pyrrole. Due to the dead time, we expect only C_{13} containing parent ions to be detected when no C_{12} -only containing parent ion was detected before. Taken into account the ion rate per shot provided for pyrrole, results in a dead time corrected relative peak height for its isotopologue of $(1 - 0.8688) \cdot 0.045 = 0.6\%$. This is in the noise level of the pyrrole peak. For the doubly charged parent, ion the isotopologue peak is present in Figure 2. Here, we only have a detection rate per shot given by 0.1073. The rate for the corresponding isotopologue peak is given by 0.00381. This gives rise to a corresponding C_{13} containing fraction of 3.4% close to the estimate provided above. The same arguments hold for the observed isotopologue peaks in the case of pyrrole-water Figure 3. Here, due to lower count rates, the isotopologue peaks are present for $\text{C}_4\text{H}_5\text{N}^+$ and $\text{C}_4\text{H}_5\text{N}(\text{H}_2\text{O})^+$.

Parent molecule	Ion	N_{det}	N_{shots}	R_{det}	$P_{\lambda}(0)$	λ	N_{real}
pyrrole	pyrrole ⁺	234626	270028	0.8688	0.1312	2.0310	548485
pyrrole	fragments	241298	270028	0.89360	-	-	241298
pyrrole(H ₂ O)	pyrrole ⁺	926658	1801197	0.5144	0.4856	0.7223	1301176
pyrrole(H ₂ O)	pyrrole(H ₂ O) ⁺	152728	1801197	0.08479	0.91521	0.08860	159591
pyrrole(H ₂ O)	fragments	91799	1801197	0.05097	-	-	91799

TABLE III. Measured number of ions, probabilities, correction factors, and real number of ions.

Data and materials availability

All data needed to interpret the conclusions in the paper are provided in the paper or the Methods section. Additional data related to this paper can be requested from the authors.

Code availability

Code used for the data analysis is available from the authors upon reasonable request.

REFERENCES

* Email: sebastian.trippel@cfel.de;

Website: <https://www.controlled-molecule-imaging.org>

- [1] C. E. Crespo-Hernández, B. Cohen, P. M. Hare, and B. Kohler, Ultrafast excited-state dynamics in nucleic acids, *Chem. Rev.* **104**, 1977 (2004).
- [2] S. Lehnert, *Biomolecular Action of Ionizing Radiation* (Taylor & Francis, London, 2007).
- [3] E. Alizadeh, T. M. Orlando, and L. Sanche, Biomolecular damage induced by ionizing radiation: The direct and indirect effects of low-energy electrons on DNA, *Annu. Rev. Phys. Chem.* **66**, 379 (2015).
- [4] T. Ito, S. C. Baker, C. D. Stickley, J. G. Peak, and M. J. Peak, Dependence of the yield of strand breaks induced by γ -rays in DNA on the physical conditions of exposure: Water content and temperature, *Int. J. Radiat. Biol.* **63**, 289 (1993).
- [5] H.-K. Kim, J. Titze, M. Schöffler, F. Trinter, M. Waitz, J. Voigtsberger, H. Sann, M. Meckel, C. Stuck, U. Lenz, M. Odenweller, N. Neumann, S. Schössler, K. Ullmann-Pfleger, B. Ulrich, R. C. Fraga, N. Petridis, D. Metz, A. Jung, R. Grisenti, A. Czasch, O. Jagutzki, L. Schmidt, T. Jahnke, H. Schmidt-Böcking, and R. Dörner, Enhanced production of low energy electrons by alpha particle impact, *PNAS* **108**, 11821 (2011).
- [6] B. Boudaïffa, P. Cloutier, D. Hunting, M. A. Hues, and L. Sanche, Resonant formation of DNA strand breaks by low-energy (3 to 20 eV) electrons, *Science* **287**, 1658 (2000).
- [7] T. D. Märk and P. Scheier, Unexpected electrons, *Nat. Phys.* **6**, 82 (2010).
- [8] T. Jahnke, Interatomic and intermolecular Coulombic decay: the coming of age story, *J. Phys. B* **48**, 082001 (2015).
- [9] L. S. Cederbaum, J. Zobeley, and F. Tarantelli, Giant intermolecular decay and fragmentation of clusters, *Phys. Rev. Lett.* **79**, 4778 (1997).
- [10] F. Martin, P. D. Burrow, Z. Cai, D. Cloutier, Pand Hunting, and L. Sanche, DNA strand breaks induced by 0–4 eV electrons: The role of shape resonances, *Phys. Rev. Lett.* **93**, 068101 (2004).
- [11] C. Y. Ng, *Vacuum Ultraviolet Photoionization and Photodissociation of Molecules and Clusters* (World Scientific Publishing Co. Pte. Ltd, 1991).
- [12] B. C. Garrett, D. A. Dixon, D. M. Camaioni, D. M. Chipman, M. A. Johnson, C. D. Jonah, G. A. Kimmel, J. H. Miller, T. N. Rescigno, P. J. Rossky, S. S. Xantheas, S. D. Colson, A. H. Laufer, D. Ray, P. F. Barbara, D. M. Bartels, K. H. Becker, K. H. Bowen, S. E. Bradforth, I. Carmichael, J. V. Coe, L. R. Corrales, J. P. Cowin, M. Dupuis, K. B. Eisenthal, J. A. Franz, M. S. Gutowski, K. D. Jordan, B. D. Kay, J. A. LaVerne, S. V. Lymar, T. E. Madey, C. W. McCurdy, D. Meisel, S. Mukamel, A. R. Nilsson, T. M. Orlando, N. G. Petrik, S. M. Pimblott, J. R. Rustad, G. K. Schenter, S. J. Singer, A. Tokmakoff, L.-S. Wang, , and T. S. Zwier, Role of water in electron-initiated processes and radical chemistry: Issues and scientific advances, *Chem. Rev.* **105**, 355 (2005).
- [13] D. Lubin and E. H. Jensen, Effects of clouds and stratospheric ozone depletion on ultraviolet radiation trends, *Nature* **377**, 710 (1995).
- [14] M. A. Barstow and J. B. Holberg, *Extreme Ultraviolet Astronomy* (Cambridge University Press, Cambridge, 2003).
- [15] T. Schultz, E. Samoylova, W. Radloff, I. V. Hertel, A. L. Sobolewski, and W. Domcke, Efficient deactivation of a model base pair via excited-state hydrogen transfer, *Science* **306**, 1765 (2004).
- [16] C. Fang, R. R. Frontiera, R. Tran, and R. A. Mathies, Mapping GFP structure evolution during proton transfer with femtosecond raman spectroscopy, *Nature* **462**, 200 (2009).
- [17] D. Marx, M. E. Tuckerman, J. Hutter, and M. Parrinello, The nature of the hydrated excess proton in water, *Nature* **397**, 601 (1999).
- [18] A. Golan, K. B. Bravaya, R. Kudirka, O. Kostko, S. R. Leone, A. I. Krylov, and M. Ahmed, Ionization of dimethyluracil dimers leads to facile proton transfer in the absence of hydrogen bonds, *Nat. Chem.* **4**, 323 (2012).
- [19] D. A. Horke, H. M. Watts, A. D. Smith, E. Jager, E. Springate, O. Alexander, C. Cacho, R. T. Chapman, and R. S. Minns, Hydrogen bonds in excited state proton transfer, *Phys. Rev. Lett.* **117**, 163002 (2016).
- [20] M. Mudrich, A. C. LaForge, A. Ciavardini, P. O’Keeffe, C. Callegari, M. Coreno, A. Demidovich, M. Devetta, M. D. Fraia, M. Drabbels, P. Finetti, O. Gessner, C. Grazi-

- oli, A. Hernando, D. M. Neumark, Y. Ovcharenko, P. Piseri, O. Plekan, K. C. Prince, R. Richter, M. P. Ziemkiewicz, T. Möller, J. Eloranta, M. Pi, M. Barranco, and F. Stienkemeier, Ultrafast relaxation of photoexcited superfluid He nanodroplets, *Nat. Commun.* **11**, 112 (2020).
- [21] P. Slavíček, N. V. Kryzhevoi, E. F. Aziz, and B. Winter, Relaxation processes in aqueous systems upon x-ray ionization: Entanglement of electronic and nuclear dynamics, *J. Phys. Chem. Lett.* **7**, 234 (2016).
- [22] M. Barbatti, A. J. A. Aquino, J. J. Szymczak, D. Nachtigallová, P. Hobza, and H. Lischka, Relaxation mechanisms of UV-photoexcited DNA and RNA nucleobases, *PNAS* **107**, 21453 (2010).
- [23] J. Zobeley, R. Santra, and L. S. Cederbaum, Electronic decay in weakly bound heteroclusters: Energy transfer versus electron transfer, *J. Chem. Phys.* **115**, 5076 (2001).
- [24] X. Ren, E. Wang, A. D. Skitnevskaya, A. B. Trofimov, G. Kirill, and A. Dorn, Experimental evidence for ultrafast intermolecular relaxation processes in hydrated biomolecules, *Nat. Phys.* **79**, 1745 (2018).
- [25] T. Jahnke, H. Sann, T. Havermeier, K. Kreidi, C. Stuck, M. Meckel, M. Schöffler, N. Neumann, R. Wallauer, S. Voss, A. Czasch, O. Jagutzki, A. Malakzadeh, F. Afaneh, T. Weber, H. Schmidt-Böcking, and R. Dörner, Ultrafast energy transfer between water molecules, *Nat. Phys.* **6**, 139 (2010).
- [26] S. Xu, D. Guo, X. Ma, X. Zhu, W. Feng, S. Yan, D. Zhao, Y. Gao, S. Zhang, X. Ren, Y. Zhao, Z. Xu, A. Dorn, L. S. Cederbaum, and N. V. Kryzhevoi, Damaging intermolecular energy and proton transfer processes in alpha-particle-irradiated hydrogen-bonded systems, *Angew. Chem. Int. Ed.* **57**, 17023 (2018).
- [27] C. Richter, D. Hollas, C. M. Saak, M. Förstel, T. Miteva, M. Mucke, O. Björneholm, N. Sisourat, P. Slavicek, and U. Hergenbahn, Competition between proton transfer and intermolecular Coulombic decay in water, *Nat. Commun.* **9**, 4988 (2018).
- [28] M. Mucke, M. Braune, S. Barth, M. Förstel, T. Lischke, V. Ulrich, T. Arion, U. Becker, A. Bradshaw, and U. Hergenbahn, A hitherto unrecognized source of low-energy electrons in water, *Nat. Phys.* **6**, 143 (2010).
- [29] S. Thürmer, M. Ončák, N. Ottosson, R. Seidel, U. Hergenbahn, S. E. Bradforth, P. Slavíček, and B. Winter, On the nature and origin of dicationic, charge-separated species formed in liquid water on X-ray irradiation, *Nat. Chem.* **5**, 590 (2013).
- [30] P. Slavíček, B. Winter, L. S. Cederbaum, and N. V. Kryzhevoi, Proton-transfer mediated enhancement of non-local electronic relaxation processes in X-ray irradiated liquid water, *J. Am. Chem. Soc.* **136**, 18170 (2014).
- [31] F. Berthias, L. Feketeová, H. Chermette, V. Forquet, C. Morell, H. Abdoul-Carime, B. Farizon, M. Farizon, and T. D. Märk, Proton Migration in Clusters Consisting of Protonated Pyridine Solvated by Water Molecules, *Chem. Phys. Chem.* **16**, 3151 (2015).
- [32] B. Liu, S. Brøndsted Nielsen, P. Hvelplund, H. Zettergren, H. Cederquist, B. Manil, and B. A. Huber, Collision-induced dissociation of hydrated adenosine monophosphate nucleotide ions: Protection of the ion in water nanoclusters, *Phys. Rev. Lett.* **97**, 133401 (2006).
- [33] N. J. Kim, Y. S. Kim, G. Jeong, T. K. Ahn, and S. K. Kim, Hydration of DNA base cations in the gas phase, *Int. J. Mass Spectrom.* **219**, 11 (2002).
- [34] B. Barc, M. Ryszka, J.-C. Pouilly, E. Jabbour Al Maalouf, Z. el Otell, J. Tabet, R. Parajuli, P. van der Burgt, P. Limao-Vieira, P. Cahillane, M. Dampc, N. Mason, and S. Eden, Multi-photon and electron impact ionisation studies of reactivity in adenine-water clusters, *Int. J. Mass Spectrom.* **365**, 194 (2014).
- [35] R. Pandey, M. Lalande, M. Ryszka, P. Limão-Vieira, N. J. Mason, J.-C. Pouilly, and S. Eden, Stabilities of nanohydrated thymine radical cations: insights from multiphoton ionization experiments and ab initio calculations, *Eur. Phys. J. D* **71**, 190 (2017).
- [36] S. K. Kim, W. Lee, and D. R. Herschbach, Cluster beam chemistry: Hydration of nucleic acid bases; ionization potentials of hydrated adenine and thymine, *J. Phys. Chem.* **100**, 7933 (1996).
- [37] J. Kočíšek, A. Pysanenko, M. Fárník, and J. Fedor, Microhydration prevents fragmentation of uracil and thymine by low-energy electrons, *J. Phys. Chem. Lett.* **27**, 3401 (2016).
- [38] E. Wang, X. Ren, W. Baek, H. Rabus, T. Pfeifer, and A. Dorn, Water acting as a catalyst for electron-driven molecular break-up of tetrahydrofuran, *Nat. Commun.* **11**, 2194 (2020).
- [39] L. F. Sukhodub, Interactions and hydration of nucleic acid bases in a vacuum. Experimental study, *Chem. Rev.* **87**, 589 (1987).
- [40] M. Neustetter, M. Mahmoodi-Darian, and S. Denifl, Study of Electron Ionization and Fragmentation of Non-hydrated and Hydrated Tetrahydrofuran Clusters, *J. Am. Soc. Mass Spectrom.* **28**, 866 (2017).
- [41] Z.-H. Loh, G. Doumy, C. Arnold, L. Kjellsson, S. H. Southworth, A. Al Haddad, Y. Kumagai, M.-F. Tu, P. J. Ho, A. M. March, R. D. Schaller, M. S. Bin Mohd Yusof, T. Debnath, M. Simon, R. Welsch, L. Inhester, K. Khalili, K. Nanda, A. I. Krylov, S. Moeller, G. Coslovich, J. Koralek, M. P. Minitti, W. F. Schlotter, J.-E. Rubensson, R. Santra, and L. Young, Observation of the fastest chemical processes in the radiolysis of water, *Science* **367**, 179 (2020).
- [42] V. Svoboda, R. Michiels, A. C. LaForge, J. Med, F. Stienkemeier, P. Slavíček, and H. J. Wörner, Real-time observation of water radiolysis and hydrated electron formation induced by extreme-ultraviolet pulses, *Science Advances* **6**, eaaz0385 (2020).
- [43] B. D. Michael and P. O'Neill, A sting in the tail of electron tracks, *Science* **187**, 1603 (2000).
- [44] C.-R. Wang, J. Nguyen, and Q.-B. Lu, Bond breaks of nucleotides by dissociative electron transfer of nonequilibrium prehydrated electrons: A new molecular mechanism for reductive DNA damage, *J. Am. Chem. Soc.* **131**, 11320 (2009).
- [45] X. Bao, J. Wang, J. Gu, and J. Leszczynski, DNA strand breaks induced by near-zero-electronvolt electron attachment to pyrimidine nucleotides, *PNAS* **103**, 5658 (2006).
- [46] J. Ma, F. Wang, S. A. Denisov, A. Adhikary, and M. Mostafavi, Reactivity of prehydrated electrons toward nucleobases and nucleotides in aqueous solution, *Science Advances* **3**, 1 (2017).
- [47] J. Ma, A. Kumar, Y. Muroya, S. Yamashita, T. Sakurai, S. A. Denisov, M. D. Sevilla, A. Adhikary, S. Seki, and M. Mostafavi, Observation of dissociative quasi-free electron attachment to nucleoside via excited anion radical in solution, *Nat. Commun.* **6**, 1 (2019).

- [48] J. Gu, J. Leszczynski, and H. F. Schaefer, Interactions of electrons with bare and hydrated biomolecules: From nucleic acid bases to DNA segments, *Chem. Rev.* **112**, 5603 (2012).
- [49] M. Smyth, J. Kohanoff, and I. I. Fabrikant, Electron-induced hydrogen loss in uracil in a water cluster environment, *J. Chem. Phys.* **140**, 184313 (2014).
- [50] A. R. Milosavljević, V. Z. Cerovski, F. Canon, M. L. Ranković, N. Škoro, L. Nahon, and A. Giuliani, Energy-dependent UV photodissociation of gas-phase adenosine monophosphate nucleotide ions: The role of a single solvent molecule, *J. Phys. Chem. Lett.* **5**, 1994 (2014).
- [51] A. T. Ulijasz, G. Cornilescu, C. C. Cornilescu, J. Zhang, M. Rivera, J. L. Markley, and R. D. Vierstra, Structural basis for the photoconversion of a phytochrome to the activated Pfr form, *Nature* **463**, 250 (2010).
- [52] M. N. R. Ashfold, B. Cronin, A. L. Devine, R. N. Dixon, and M. G. D. Nix, The role of $\pi\sigma^*$ excited states in the photodissociation of heteroaromatic molecules, *Science* **312**, 1637 (2006).
- [53] A. L. Sobolewski, W. Domcke, C. Dedonder-Lardeux, and C. Jouvet, Excited-state hydrogen detachment and hydrogen transfer driven by repulsive $^1\pi\sigma^*$ states: A new paradigm for nonradiative decay in aromatic biomolecules, *Phys. Chem. Chem. Phys.* **4**, 1093 (2002).
- [54] A. L. Sobolewski and W. Domcke, Conical intersections induced by repulsive $^1\pi\sigma^*$ states in planar organic molecules: malonaldehyde, pyrrole and chlorobenzene as photochemical model systems, *Chem. Phys.* **259**, 181 (2000).
- [55] H. Lippert, V. Stert, L. Hesse, C. P. Schulz, I. V. Hertel, and W. Radloff, Ultrafast photoinduced processes in indole-water clusters, *Chem. Phys. Lett.* **376**, 40 (2003).
- [56] A. L. Sobolewski and W. Domcke, Photoejection of electrons from pyrrole into an aqueous environment: ab initio results on pyrrole-water clusters, *Chem. Phys. Lett.* **321**, 479 (2000).
- [57] T. M. Korter, D. W. Pratt, and J. Küpper, Indole-H₂O in the gas phase. Structures, barriers to internal motion, and S₁ ← S₀ transition moment orientation. Solvent reorganization in the electronically excited state, *J. Phys. Chem. A* **102**, 7211 (1998).
- [58] S. K. Pal, J. Peon, and A. H. Zewail, Biological water at the protein surface: Dynamical solvation probed directly with femtosecond resolution, *PNAS* **99**, 1763 (2002).
- [59] J. Onvlee, S. Trippel, and J. Küpper, Ultrafast light-induced dynamics in solvated biomolecules: The indole chromophore with water, *Nat. Commun.* **13**, 7462 (2022), arXiv:2103.07171 [physics].
- [60] W. Domcke and A. L. Sobolewski, Spectroscopy meets theory, *Nat. Chem.* **5**, 257 (2013).
- [61] M. J. Tubergen, A. M. Andrews, and R. L. Kuczkowski, Microwave spectrum and structure of a hydrogen-bonded pyrrole-water complex, *J. Phys. Chem.* **97**, 7451 (1993).
- [62] G. M. Roberts, C. A. Williams, H. Yu, A. S. Chatterley, J. D. Young, S. Ullrich, and V. G. Stavros, Probing ultrafast dynamics in photoexcited pyrrole: timescales for $^1\pi\sigma^*$ mediated H-atom elimination, *Faraday Disc.* **163**, 95 (2013).
- [63] O. M. Kirkby, M. A. Parkes, S. P. Neville, G. A. Worth, and H. H. Fielding, Non-radiative relaxation dynamics of pyrrole following excitation in the range 249.5–200 nm, *Chem. Phys. Lett.* **683**, 179 (2017).
- [64] H. Lippert, H.-H. Ritze, I. V. Hertel, and W. W. Radloff, Femtosecond time-resolved hydrogen-atom elimination from photoexcited pyrrole molecules, *Chem. Phys. Lett.* **5**, 1423 (2004).
- [65] K. Grygoryeva, J. Rakovský, I. Vinklárček, O. Votava, M. Fárník, , and V. Poterya, Vibrationally mediated photodissociation dynamics of pyrrole, *AIP Adv.* **9**, 0351511 (2019).
- [66] I. Frank and K. Damianos, Excited state dynamics in pyrrole-water clusters: First principles simulation, *Chem. Phys.* **343**, 347 (2008).
- [67] A. J. van den Brom, M. Kapelios, T. N. Kitsopoulos, N. H. Nahler, B. Cronin, and M. N. R. Ashfold, Photodissociation and photoionization of pyrrole following the multiphoton excitation at 243 and 364.7 nm, *Phys. Chem. Chem. Phys.* **7**, 5704 (2005).
- [68] E. Rennie, C. Johnson, J. Parker, R. Ferguson, D. Holland, and D. Shaw, A photoabsorption and mass spectrometry study of pyrrole, *Chem. Phys.* **250**, 217 (1999).
- [69] M. Schütz, Y. Matsumoto, A. Bouchet, M. Öztürk, and O. Dopfer, Microsolvation of the pyrrole cation (Py⁺) with nonpolar and polar ligands: infrared spectra of Py⁺-L_n with L = Ar, N₂, and H₂O (*n* ≤ 3), *Phys. Chem. Chem. Phys.* **15**, 3970 (2017).
- [70] M. Johny, J. Onvlee, T. Kierspel, H. Bieker, S. Trippel, and J. Küpper, Spatial separation of pyrrole and pyrrole-water clusters, *Chem. Phys. Lett.* **721**, 149–152 (2019), arXiv:1901.05267 [physics].
- [71] A. Zhao, M. van Beuzekom, B. Bouwens, D. Byelov, I. Chakaberia, C. Cheng, E. Maddox, A. Nomerotski, P. Svihra, J. Visser, V. Vrba, and T. Weinacht, Coincidence velocity map imaging using Tpx3Cam, a time stamping optical camera with 1.5 ns timing resolution, *Rev. Sci. Instrum.* **88**, 113104 (2017), arXiv:1707.06253 [physics].
- [72] A. Al-Refai, M. Johny, J. Correa, D. Pennicard, P. Svihra, A. Nomerotski, S. Trippel, and J. Küpper, PymePix: A python library for SPIDR readout of Timepix3, *J. Instrum.* **14** (10), P10003, arXiv:1905.07999 [physics].
- [73] H. Bromberger, C. Passow, D. Pennicard, R. Boll, J. Correa, L. He, M. Johny, C. Papadopoulou, A. Tul-Noor, J. Wiese, S. Trippel, B. Erk, and J. Küpper, Shot-by-shot 250 kHz 3D ion and MHz photoelectron imaging using Timepix3, *J. Phys. B* **55**, 144001 (2022), arXiv:2111.14407 [physics].
- [74] V. Profant, V. Poterya, M. Fárník, P. Slavíček, and U. Buck, Fragmentation dynamics of size-selected pyrrole clusters prepared by electron impact ionization: Forming a solvated dimer ion core, *J. Phys. Chem. A* **111**, 12477 (2007).
- [75] H. Bieker, J. Onvlee, M. Johny, L. He, T. Kierspel, S. Trippel, D. A. Horke, and J. Küpper, Pure molecular beam of water dimer, *J. Phys. Chem. A* **123**, 7486 (2019), arXiv:1904.08716 [physics].
- [76] M. H. Palmer, I. C. Walker, and M. F. Guest, The electronic states of pyrrole studied by optical (VUV) absorption, near-threshold electron energy-loss (EEL) spectroscopy and ab initio multi-reference configuration interaction calculations, *Chem. Phys.* **238**, 179 (1998).
- [77] P. J. Derrick, L. Åsbrink, O. Edqvist, B. Å. Jonsson, and E. Lindholm, Rydberg series in small molecules: XII. photoelectron spectroscopy and electronic structure of pyrrole, *Int. J. Mass Spectrom. Ion Physics* **6**, 191 (1971).
- [78] G. D. Willett and T. Baer, Thermochemistry and dissociation dynamics of state-selected C₄H₄X ions. 3. C₄H₅N⁺, *J. Am. Chem. Soc.* **102**, 6774 (1980).

- [79] I. V. Hertel and W. Radloff, Ultrafast dynamics in isolated molecules and molecular clusters, *Rep. Prog. Phys.* **69**, 1897 (2006).
- [80] S. Trippel, T. G. Mullins, N. L. M. Müller, J. S. Kienitz, K. Długołęcki, and J. Küpper, Strongly aligned and oriented molecular samples at a kHz repetition rate, *Mol. Phys.* **111**, 1738 (2013), arXiv:1301.1826 [physics].
- [81] Y.-P. Chang, D. A. Horke, S. Trippel, and J. Küpper, Spatially-controlled complex molecules and their applications, *Int. Rev. Phys. Chem.* **34**, 557 (2015), arXiv:1505.05632 [physics].
- [82] A. Roberts, P. Svihra, A. Al-Refaie, H. Graafsma, J. Küpper, K. Majumdar, K. Mavrokoridis, A. Nomerotski, D. Pennicard, B. Philippou, S. Trippel, C. Touramanis, and J. Vann, First demonstration of 3D optical readout of a TPC using a single photon sensitive Timepix3 based camera, *J. Instrum.* **14** (06), P06001, arXiv:1810.09955 [physics].
- [83] S. Hankin, D. Villeneuve, P. Corkum, and D. Rayner, Intense-field laser ionization rates in atoms and molecules, *Phys. Rev. A* **64**, 013405 (2001).
- [84] J. Wiese, J.-F. Olivieri, A. Trabattoni, S. Trippel, and J. Küpper, Strong-field photoelectron momentum imaging of OCS at finely resolved incident intensities, *New J. Phys.* **21**, 083011 (2019), arXiv:1904.07519 [physics].
- [85] R. H. Page, Y. R. Shen, and Y. T. Lee, High-resolution photoionization spectrum of water molecules in a supersonic beam, *J. Chem. Phys.* **88**, 5362 (1988).
- [86] S. V. Popruzhenko, Keldysh theory of strong field ionization: history, applications, difficulties and perspectives, *J. Phys. B* **47**, 204001 (2014).

Acknowledgments

We thank Jolijn Onvlee, Jonathan Correa, and David Pennicard for helpful discussions.

Funding

We acknowledge financial support by Deutsches Elektronen-Synchrotron DESY, a member of the Helmholtz Association (HGF), the European Union’s Horizon 2020 research and innovation program under the Marie Skłodowska-Curie Grant Agreement 641789 “Molecular Electron Dynamics investigated by Intense Fields and Attosecond Pulses” (MEDEA), the Clusters of Excellence “Center for Ultrafast Imaging” (CUI, EXC 1074, ID 194651731) and “Advanced Imaging of Matter” (AIM, EXC 2056, ID 390715994) of the Deutsche Forschungsgemeinschaft (DFG), and the European Research Council under the European Union’s Seventh Framework Programme (FP7/2007-2013) through the Consolidator Grant COMOTION (614507). We acknowledge the use of the Maxwell computational resources operated at Deutsches Elektronen-Synchrotron DESY, Hamburg, Germany.

Author contributions

M.J., S.T., and J.K. conceived the experiment; M.J., C.S., A.R., L.H., and S.T. performed the experiment; A.R. adopted the pymepix software; M.J. and S.T. analysed the data; M.J., J.W., S.T., and J.K. interpreted the results; M.J., S.T., and J.K. prepared the manuscript. All authors discussed the results and the manuscript.

Competing interests

The authors declare that they have no competing interests.